https://doi.org/10.5194/ms-2026-201
Preprint. Discussion started: 20 November 2026
© Author(s) 2026. CC BY 4.0 License.



mechanical sciences
DISCUSSIONS

Coupled skidding–impact dynamics of angular contact ball bearings with localized outer ring defects under elastohydrodynamic lubrication

Baiwei Xue, Chunli Lei, Guangyi Ren, Mingjun Jia, Weili Zhao, and Xiwen Zhang

School of Mechanical and Electrical Engineering, Lanzhou University of Technology, Lanzhou, Gansu 730050, China

Corresponding author: Lei Chunli (e-mail: lclyq2004@163.com)

Abstract: Localized outer-race defects in angular contact ball bearings (ACBBs) can generate impact excitation, while rolling-element skidding alters the kinematic conditions at the contact interfaces. This study investigates their coupled effects on bearing response in the presence of elastohydrodynamic lubrication (EHL). A dynamic model with four degrees of freedom is developed by incorporating spinning motion, lubricant-film effects, rolling-element skidding, and impact-related velocity variations. The modeling procedure begins with the formulation of a time-dependent displacement function to represent the excitation associated with a localized defect. The effective bearing stiffness is then evaluated through the integration of the Hertzian contact contribution and the stiffness provided by the lubricant film. To characterize non-ideal rolling behavior, the skidding velocities relative to the inner and outer races are determined by accounting for rolling-element motion and the transient velocity changes associated with interactions at the defect boundaries. The corresponding friction forces are subsequently incorporated into the dynamic equations. Numerical results indicate that spinning motion reduces the vibration amplitude, whereas EHL provides a pronounced attenuation of bearing vibration. An increase in rotational speed leads to higher fault-related characteristic frequencies and vibration amplitudes. In contrast, skidding lowers the characteristic frequency while intensifying the vibration response. When defect-edge impacts are included, the resulting transient increase in rolling-element velocity produces a higher characteristic frequency than that predicted by the model considering skidding alone, accompanied by a further increase in vibration amplitude. Variations in defect size and applied load affect the vibration amplitude but do not change the fault characteristic frequency.

Keywords: angular contact ball bearings; outer-race defect; elastohydrodynamic lubrication; skidding; impact-induced vibration.

1. Introduction

Angular contact ball bearings (ACBBs) are commonly employed in aerospace systems, railway transportation, robotics, and other rotating machinery because of their ability to support shaft systems and maintain accurate rotational motion (Cao et al., 2018). During service, however, complex loading conditions and demanding operating environments may cause localized damage, including cracks, pits, and spalling. Such damage changes the local contact geometry and alters how rolling elements engage with the raceways. As a rolling element passes through a damaged region, variations in contact conditions may generate transient impacts and increase the vibration level of the bearing assembly. In addition to localized damage, rolling-element skidding introduces relative motion at the contact interfaces, which can impair lubrication, compromise operating accuracy, accelerate wear, and reduce bearing service life (Evans et al., 2013; Tu et al., 2024; Xu et al., 2025).

https://doi.org/10.5194/ms-2026-201
Preprint. Discussion started: 20 November 2026
© Author(s) 2026. CC BY 4.0 License.



mechanical sciences
DISCUSSIONS

Therefore, understanding the coupled dynamic behavior of ACBBs with localized outer-race defects is important for improving operational reliability and clarifying the mechanisms underlying bearing faults.

Extensive research has focused on modeling the vibration behavior of rolling bearings containing localized defects. Existing approaches differ mainly in how defect shape, contact states, and excitation arising from impacts are represented. For example, Patel et al. (2010) employed a sinusoidal function to describe defect-related displacement excitation and examined its influence on bearing vibration. Yan et al. (2018) modeled a localized defect as a rectangular crack and formulated a two-degree-of-freedom model for deep-groove ball bearings using Hertzian contact theory. Subsequent studies have explored more detailed descriptions of defect-induced excitation. Li et al. (2022) formulated an impact-force function to investigate interactions between rolling elements and the edges of an outer-race defect, whereas Shang et al. (2023) established a dynamic model for rolling bearings with gradually evolving inner-race defects, considering defect morphology, radial load, and rolling-element skidding. Wen et al. (2021) examined the effects of defect dimensions using a model with multiple degrees of freedom for ACBBs. To more accurately characterize fault excitation, Li et al. (2020) and Qin et al. (2020) adopted B-spline-based fitting techniques, while Wu et al. (2022) developed a displacement excitation function that accounts for localized damage. Yan et al. (2020) established a five-degree-of-freedom model and analyzed variations in oil-film stiffness, overall bearing stiffness, and vibration response under different rotational speeds and loads. Luo et al. (2019) incorporated time-varying contact stiffness associated with inner-race spalling into a dynamic model of ACBBs. Zhang et al. (2021) accounted for radial clearance and time-dependent excitation in a bearing model with two degrees of freedom and inner-race defects, evaluating how defect width, radial load, and rotational speed affect fault-related signal characteristics. The role of transient impacts has also been investigated. Jiang et al. (2019) developed an improved dynamic model considering the three-dimensional geometric relationship between rolling elements and defect areas, and investigated the resulting changes in contact force and vibration response, while Niu et al. (2014) analyzed ball-bearing responses in both the time and frequency domains under localized raceway damage. More recently, Li et al. (2026) investigated defective-bearing dynamics while accounting for fluid–structure interaction. Although these studies have advanced the modeling of defect-related excitation and vibration, the interaction between localized damage and rolling-element skidding remains insufficiently addressed in the context considered here.

Skidding in rolling bearings has also attracted considerable research attention. Harris (1971) developed an analytical approach for predicting skidding in thrust-loaded angular-contact ball bearings. Dawoud et al. (2023) investigated how structural parameters and operating conditions influence skidding behavior, while Han et al. (2018) proposed a nonlinear dynamic formulation for cylindrical roller bearings incorporating radial clearance, Hertzian contact, and elastohydrodynamic lubrication (EHL), and experimentally assessed its accuracy. Dadouche and Kerrouche (2022) examined the relationship between radial loading and roller skidding and discussed its implications for bearing performance. For ACBBs, Jain and Hunt (2011) developed a dynamic model for evaluating skidding under radial loading while considering spinning motion and lubrication. Wang et al. (2015) investigated how loading conditions affect skidding in bearings, and Bao et al. (2024) presented an analytical approach for characterizing rolling-element skidding under radial load. Zhao et al. (2023) further investigated the role of loading and rolling-contact effects in the skidding behavior of ACBBs. In addition, Tu et al. (2021) developed a nonlinear dynamic model of

https://doi.org/10.5194/ms-2026-201
Preprint. Discussion started: 20 November 2026
© Author(s) 2026. CC BY 4.0 License.



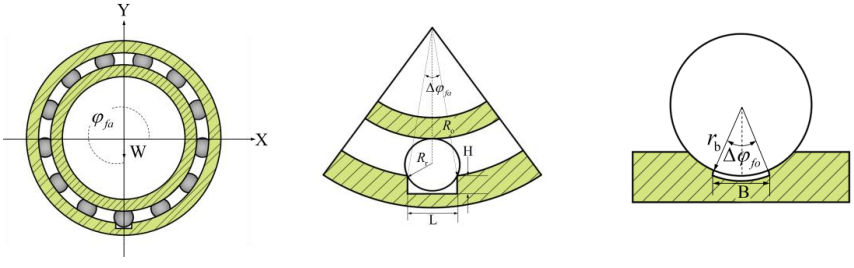
mechanical sciences DISCUSSIONS

cylindrical roller bearings considering skidding and incorporated frictional and contact forces to investigate their effects on bearing vibration. Nevertheless, the combined effects of skidding, defect-edge impacts, and EHL in bearings with localized outer-race damage remain to be explored in greater depth.

To bridge this gap, the present study develops a four-degree-of-freedom dynamic model for ACBBs with a localized outer-race defect, incorporating skidding, spinning motion, EHL, and impact-induced velocity variations. First, a time-dependent displacement excitation function is formulated to describe the passage of rolling elements through a rectangular defect. The effective bearing stiffness is then obtained by considering both the Hertzian contact stiffness and the stiffness contributed by the lubricant film while accounting for rolling-element spin. Subsequently, the skidding speeds relative to the inner and outer raceways are derived by considering rolling-element motion and the velocity changes associated with collisions at the defect boundaries. These velocities are used to calculate friction forces, which are included in the governing equations of bearing motion. Finally, the developed model is employed to assess how rotational speed, skidding, defect geometry, and applied load affect the vibration response and fault-related characteristic frequency.

2. Local defect-induced excitation model

As a rolling element moves across a damaged section of the outer raceway, its displacement changes progressively during entry into and exit from the defect. This variation in displacement over time is represented by a time-dependent excitation function. For the purposes of geometric modeling, the outer-race defect is assumed to have a rectangular profile, as shown in Fig. 1.



(a) Overall model (b) circumferential dimension of defect (c) Defect axial dimension

Figure 1. Geometric representation of local defects in ball bearings

In Fig. 1, the azimuth angle of the defect center is denoted by φ_{fa}, $\Delta\varphi_{fa}$ is the circumferential span angle, and $\Delta\varphi_{fo}$ is the axial span angle. R_r denotes the rolling-element radius, while R_o and r_b represent the radii of curvature of the outer ring and outer raceway, respectively. W represents the applied load, whereas H, L, and B indicate the defect depth, length, and width, respectively.

With the cage at its reference position, the azimuth angle of the j-th rolling element is given by

$$\varphi_j = \omega_{cag} t + \frac{2\pi(j-1)}{N}, j = 1 \sim N \tag{1}$$

where ω_{cag} is the cage speed, and N is the total number of rolling elements.

The contact depth associated with the interaction between the rolling element and the defect shown in Fig. 1(b) is determined using Eq. (2) (Lei et al., 2025):

https://doi.org/10.5194/ms-2026-201
Preprint. Discussion started: 20 November 2026
© Author(s) 2026. CC BY 4.0 License.



mechanical sciences DISCUSSIONS

$$d(\varphi)_1 = \begin{cases} \min\{\mathrm{H}, R_\mathrm{r} - \sqrt{[R_\mathrm{r}^2 - 0.25R_\mathrm{o}^2(\varphi_j - \varphi_{fa} + 0.5\Delta\varphi_{fa})]}\} \\ \varphi_{fa} - \dfrac{1}{2}\Delta\varphi_{fa} < \varphi_j < \varphi_{fa} \\ \min\{\mathrm{H}, R_\mathrm{r} - \sqrt{[R_\mathrm{r}^2 - 0.25R_\mathrm{o}^2(\varphi_{fa} - \varphi_j + 0.5\Delta\varphi_{fa})]}\} \\ \varphi_{fa} < \varphi_j < \varphi_{fa} + \dfrac{1}{2}\Delta\varphi_{fa} \end{cases} \tag{2}$$

The contact depth of the rolling element within the defect illustrated in Fig. 1(c) is defined by Eq. (3):

$$d(\varphi)_2 = r_\mathrm{b} + \sqrt{r_\mathrm{b}^2 - [r_\mathrm{b}\sin(0.5\Delta\varphi_{fo})]^2} - \sqrt{R_\mathrm{r}^2 - [r_\mathrm{b}\sin(0.5\Delta\varphi_{fo})]^2} \tag{3}$$

Based on these relationships, the excitation function describing displacement variations over time for the rectangular defect is derived as:

$$H_d = \begin{cases} \min(\mathrm{H}, d(\varphi)_1, d(\varphi)_2)\ ,\ if\ \ \varphi_{fa} - \dfrac{1}{2}\Delta\varphi_{fa} < \varphi_j < \varphi_{fa} + \dfrac{1}{2}\Delta\varphi_{fa} \\ 0, else \end{cases} \tag{4}$$

3. Comprehensive stiffness modeling for rolling bearings

3.1 Contact stiffness

For point contact between a healthy raceway and a rolling element, the load-deflection relationship is described as:

$$Q_c = K_n\delta^{\frac{3}{2}} \tag{5}$$

where Q_c is the contact load, K_n denotes the load-deflection coefficient, and δ represents the elastic deformation.

The load acting in the defective region is determined by subtracting the load relieved by the defect from the contact load that would act between the rolling element and the intact raceway. Accordingly, the contact load for the defective region is expressed as (Lei et al., 2025):

$$Q_d = Q_c - \iint_D \frac{3Q_c}{2\pi ab}\left[1 - \left(\frac{x}{a_H}\right)^2 - \left(\frac{y}{b_H}\right)^2\right]^{\frac{1}{2}} \mathrm{dxdy} \tag{6}$$

where a_H and b_H are the semi-major and semi-minor axes, respectively, of the normal contact ellipse under the normal load applied to the healthy raceway. The double integral accounts for the load associated with the defective portion, with the integration domain D specified as follows:

$$\left\{(x,y)\middle| \begin{array}{c} x \in \left[-\frac{1}{2}r_\mathrm{b}\Delta\varphi_{fo}, \frac{1}{2}r_\mathrm{b}\Delta\varphi_{fo}\right] \\ y \in \left[R_\mathrm{o}\left(-\varphi_j + \varphi_{fa} - \frac{1}{2}\Delta\varphi_{fa}\right), R_\mathrm{o}\left(-\varphi_j + \varphi_{fa} + \frac{1}{2}\Delta\varphi_{fa}\right)\right] \end{array}\right\} \tag{7}$$

From Equations (5)-(7), the contact stiffness associated with the defective outer raceway can be written as:

$$K_\mathrm{o}(\varphi_j) = \lim_{\delta\to 0}\frac{Q_d}{\delta} \tag{8}$$

3.2 Film thickness and stiffness model

Considering the kinematic description of spinning in ACBBs, the motion can be represented by an ellipsoid translating over an infinite plane with the mean velocity u_b of the rolling element relative to the raceway, while the plane rotates with an angular spin velocity ω_s, as shown in Fig. 2 (Lei et al., 2020). The velocity components at any point on the plane are represented by v_R and u_R, respectively.

https://doi.org/10.5194/ms-2026-201
Preprint. Discussion started: 20 November 2026
© Author(s) 2026. CC BY 4.0 License.



mechanical sciences
DISCUSSIONS

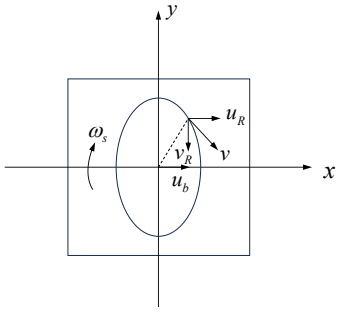


Figure 2. Spin motion model

The velocity components v_R and u_R at an arbitrary point can be determined from the spin motion model in Fig. 2 as follows:

$$\begin{cases} u_R(x,y) = \dfrac{\omega_s y}{2} + u_b \\ v_R(x,y) = -\dfrac{\omega_s x}{2} \end{cases} \tag{9}$$

where ω_s is separated into the inner-ring and outer-ring spin angular velocities, ω_{si} and ω_{so} respectively. These quantities are expressed as follows:

$$\begin{cases} \omega_{si} = \omega_r \sin(\alpha_i - \beta) - (\omega_i - \omega_m)\sin\alpha_i \\ \omega_{so} = \omega_r \sin(\alpha_o - \beta) - \omega_m \sin\alpha_o \end{cases} \tag{10}$$

where ω_r characterizes the rolling element's self-spinning motion, whereas ω_m represents its revolution angular velocity. The contact angles at the inner and outer rings are denoted by α_i and α_o respectively, while β denotes the element's angular orientation.

3.2.1 Lubricant-film thickness

With spinning motion taken into account, the minimum lubricant-film thickness is expressed as (Lei et al., 2024):

$$H_{\min s} = 8.9\times10^{-3} U^{0.72}\left(1+1.043e^{-664.016W}\right)G^{0.8001}k^{1.616}\cdot \left(1+21.459e^{-0.3k}\right)\left(1-13101\times10^{10}\Omega_s^{1.024}\right) \tag{11}$$

where U refers to entrainment velocity, G defines the material parameter, Ω_s represents spin velocity parameter, k denotes the ellipticity. The ranges of values for these parameters are listed in Table 1.

Table 1 Parameter value ranges

Parameter	Value
U	1.68×10^{-11}~6.74×10^{-10}
G	2500~5000
Ω_s	0~4.41×0^{-11}
k	1~9.5

The minimum oil film thickness between the rolling element and the raceway is represented

https://doi.org/10.5194/ms-2026-201
Preprint. Discussion started: 20 November 2026
© Author(s) 2026. CC BY 4.0 License.



mechanical sciences DISCUSSIONS

as:

$$h_{\min s} = R_x \times H_{\min s} \tag{12}$$

where R_x represents the equivalent radius of curvature of the two contacting along the x direction.

3.2.2 Equation for film stiffness

The oil film stiffness under spinning motion is determined from the dependence of minimum oil film thickness on load and the definition of oil film stiffness, as follows:

$$K_f = -\frac{dw_{films}}{dh_{\min s}} \tag{13}$$

where the detailed calculation is referred to Li et al. (2020).

3.3 Stiffness model

During ACBB operation, the overall stiffness is determined by both the Hertz contact stiffness $K_{\mathrm{i}} / K_{\mathrm{o}}(\varphi_j)$ and oil film stiffness K_{fi} / K_{fo} considering spin motion, with spinning motion taken into account. The stiffnesses associated with the inner and outer rings, represented by K_{ci} and K_{co}, respectively, are obtained by combining the corresponding Hertz contact stiffness and lubricant-film stiffness in series:

$$\begin{cases} K_{ci} = \dfrac{K_{\mathrm{i}} K_{fi}}{K_{\mathrm{i}} + K_{fi}} \\ K_{co} = \dfrac{K_{\mathrm{o}}(\varphi_j) K_{fo}}{K_{\mathrm{o}}(\varphi_j) + K_{fo}} \end{cases} \tag{14}$$

The overall bearing stiffness K_c is subsequently calculated by combining K_{ci} and K_{co} in series, and is expressed as:

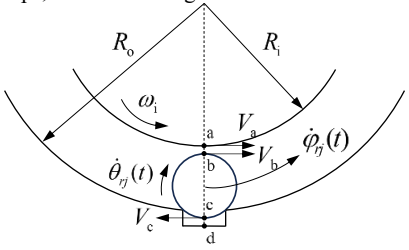
$$K_c = \frac{K_{co} K_{ci}}{K_{co} + K_{ci}} \tag{15}$$

4. Fault dynamics model for ACBBs considering skidding and impact effects

To precisely characterize the dynamic behavior of ACBBs, the model accounts for outer-ring defects under skidding conditions, considering EHL and spinning motion, rolling element skidding and impact effects at the defect are introduced and a relative velocity model is developed, then a friction force equation based on skidding velocity is derived. Subsequently, the friction force is introduced into the equations of motion to develop a dynamic model of defective bearings under skidding conditions. This model enables the coupled effects of skidding, impact, and lubrication on bearing vibration characteristics to be examined.

4.1 Calculation of relative skidding velocity

The relative skidding velocity between the *j*-th rolling element and the raceway is obtained from their kinematic relationships, as shown in Fig. 3.



https://doi.org/10.5194/ms-2026-201
Preprint. Discussion started: 20 November 2026
© Author(s) 2026. CC BY 4.0 License.



mechanical sciences DISCUSSIONS

Figure 3. Relative skidding velocity relationship

Upon entering the damaged region, the rolling element's velocity at point a depends on the inner ring's angular velocity and the corresponding rotation radius. Hence, the linear velocity at point a is obtained as:

$$V_{\mathrm{a}} = \omega_{\mathrm{i}} R_{\mathrm{i}} \tag{16}$$

where R_{i} represents the curvature radius of the inner ring.

As the rolling element travels around the center of the outer raceway while spinning about its own center, the linear velocity at point b is given by the sum of its orbital linear velocity and rotational linear velocity, expressed as:

$$V_{\mathrm{b}} = (R_{\mathrm{i}} + H_d)\dot{\varphi}_{rj}(t) + R_{\mathrm{r}}\dot{\theta}_{rj}(t) \tag{17}$$

where $\dot{\varphi}_{rj}(t)$ and $\dot{\theta}_{rj}(t)$ are the orbital rotation speed and rotation speed associated with the *j*-th rolling element, respectively.

The linear velocity at point c is given by the orbital linear velocity of the rolling element around the outer raceway center minus its rotational linear velocity, expressed as:

$$V_{\mathrm{c}} = (R_{\mathrm{o}} + H_d)\dot{\varphi}_{rj}(t) - R_{\mathrm{r}}\dot{\theta}_{rj}(t) \tag{18}$$

Since the outer ring is stationary, the linear velocity at point d is zero, expressed as:

$$V_{\mathrm{d}} = 0 \tag{19}$$

The relative skidding velocity at the contact between the rolling element and the inner ring is calculated as the difference between the linear velocities at points a and b, given by:

$$\Delta v_{\mathrm{i}sj} = V_{\mathrm{a}} - V_{\mathrm{b}} = \omega_{\mathrm{i}} R_{\mathrm{i}} - \left[(R_{\mathrm{i}} + H_d)\dot{\varphi}_{rj}(t) + R_{\mathrm{r}}\dot{\theta}_{rj}(t)\right] \tag{20}$$

The relative skidding velocity at the contact between the rolling element and the outer ring is obtained from the difference between the linear velocities at points c and d, as follows:

$$\Delta v_{\mathrm{o}sj} = V_{\mathrm{c}} - V_{\mathrm{d}} = (R_{\mathrm{o}} + H_d)\dot{\varphi}_{rj}(t) - R_{\mathrm{r}}\dot{\theta}_{rj}(t) \tag{21}$$

4.2 Relative velocity after impact

This section establishes a modified skidding velocity model considering the impact of the defect. Different from traditional dynamic models that assume pure rolling contact, this paper incorporates the velocity variations caused by orbital revolution, rotation, and collision with the defect edge into the skidding velocity expression, providing a more representative description of bearing motion under operating conditions.

As shown in Fig. 4, a rolling element passes through a defect in three stages: entering the damaged area, experiencing impact, and leaving the region.

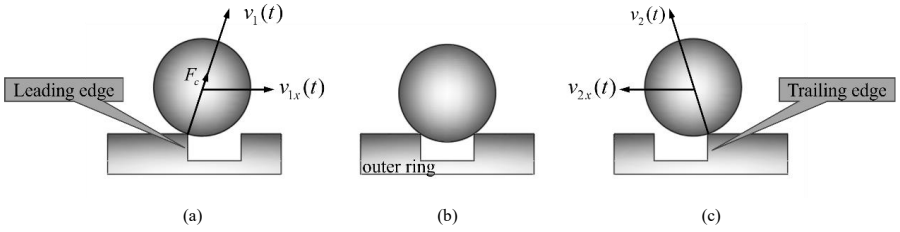


Fig. 4 Stages of rolling-element interaction with a defect

At the entry stage shown in Fig. 4(a), the presence of the defect increases the internal clearance of the bearing and reduces the contact force, thereby initiating stress release. The corresponding change in rolling-element velocity is described by:

https://doi.org/10.5194/ms-2026-201
Preprint. Discussion started: 20 November 2026
© Author(s) 2026. CC BY 4.0 License.



mechanical sciences DISCUSSIONS

$$v_1(t)=\frac{F_c}{m_r}\left(t-t_{entry}\right)+\frac{\triangle\varphi_a F_c}{\pi m_r \omega_{cage}}\left[\cos\left(\frac{\pi\omega_{cage}\left(t-t_{entry}\right)}{\triangle\varphi_a}\right)-1\right] \quad t_{entry}<t\le t_{center} \tag{22}$$

where F_c represents the contact force generated when the rolling element strikes the defect edge (Luo et al., 2019), m_r is the mass of the rolling element, and t_{entry} specifies the instant when a rolling element first enters the damaged region.

Upon reaching the center of the defect (Fig. 4(b)), the impact force acting on it attains its maximum F_{max} (Luo et al., 2019), with the time instant of entering the center position denoted as t_{center}. From this instant, the velocity change is expressed as:

$$v_2(t)=\frac{F_{max}}{m_r}\left(t-t_{center}\right)-\frac{\triangle\varphi_a F_{max}}{\pi m_r \omega_{cage}}\sin\left(\frac{\pi\omega_{cage}\left(t-t_{center}\right)}{\triangle\varphi_a}\right) \quad t_{center}\le t<t_{exit} \tag{23}$$

where t_{exit} represents the instant which the defect is exited.

Rotates about the contact point at the trailing edge. (Fig. 4(c)) until it exits the defect region. Furthermore, the impact also changes the direction of motion, and the corresponding contact geometry at the defect boundary is illustrated in Fig. 5.

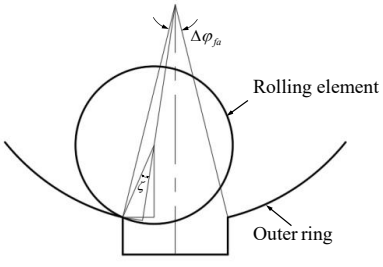


Fig. (a) Entering the defect.

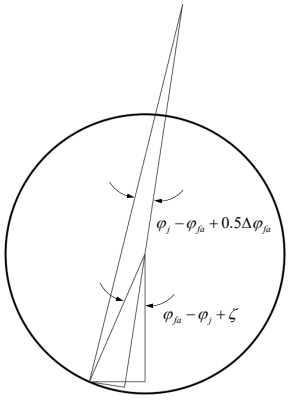


Fig. (b) Local enlarged view at the leading edge.

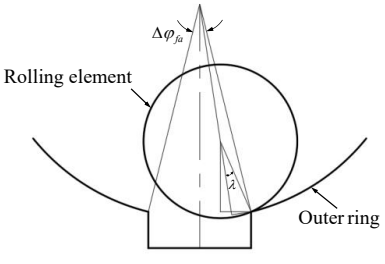


Fig. (c) Exiting the defect.

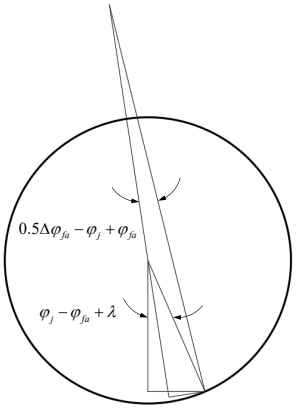


Fig. (d) Local enlarged view at the trailing edge.

Figure. 5 Schematic of impact at the defect edge

Upon entering the defect region, its velocity direction is altered due to the collision. Let ζ denote the angle between the line joining the element center to the leading edge of the defect and

https://doi.org/10.5194/ms-2026-201
Preprint. Discussion started: 20 November 2026
© Author(s) 2026. CC BY 4.0 License.



mechanical sciences DISCUSSIONS

the angular position of the element. The velocity component along x direction after the collision is expressed as:

$$v_{1x}(t) = v_1(t)\sin\left(\varphi_{fa} - \varphi_j + \zeta\right) \tag{24}$$

For the exit stage, let λ represent the angle between the line joining the element center to the defect's trailing edge and its angular position. The corresponding x direction velocity is then determined as follows:

$$v_{2x}(t) = v_2(t)\sin(\varphi_j - \varphi_{fa} + \lambda) \tag{25}$$

The contact angle α of ACBBs is also incorporated into the skidding velocity calculation. By accounting for the interaction between the two velocity components, the final expressions for the relative skidding velocities are given as follows:

$$\Delta v_{ij} = \Delta v_{isj}(t)\cos\alpha \tag{26}$$

$$\Delta v_{oj} = \begin{cases} \left[\Delta v_{osj} - v_{1x}(t)\right]\cos\alpha & t_{entry} \le t < t_{center} \\ \left[\Delta v_{osj} - v_{1x}(t) + v_{2x}(t)\right]\cos\alpha & t_{center} \le t \le t_{exit} \end{cases} \tag{27}$$

4.3 Friction force formulation

Friction plays an important role in rolling-element motion and directly affects the dynamic characteristics of rolling bearings. Its influence persists throughout bearing operation and becomes particularly significant under skidding conditions. In this study, a four-parameter friction model is adopted to evaluate the friction coefficient, following the approach commonly used in the dynamic analysis of rolling bearings (Zhang et al., 2016). The coefficient is assumed to be a function solely of the relative skidding velocity and is calculated using Eq. (28).

$$\mu = (a_1 + a_2 \mid \Delta v \mid)\exp(-a_3 \mid \Delta v \mid) + a_4 \tag{28}$$

where a_1, a_2, a_3, and a_4 are the lubricant coefficients, and their values refer to Li et al. (2015).

Considering the previously established geometric relationships and EHL, the central film thicknesses at the inner and outer ring contacts are denoted by h_{ci} and h_{co}, respectively, with their calculation methods referred to Hamrock and Dowson (1977). Accordingly, the contact deformation at the inner and outer raceways for the *j*-th element is expressed as follows:

$$\delta_{ij} = (x_1 - x_2)\cos\varphi_j + \left(y_1 - y_2\right)\sin\varphi_j - \delta_{rj} - c/2 - h_{ci} \tag{29}$$

$$\delta_{oj} = \delta_{rj} - c/2 - h_{co} - H_d\cos\alpha \tag{30}$$

where x_1 and y_1 define the position of the axis, x_2 and y_2 specify the location of the bearing housing (Lei et al., 2025), The radial displacement is denoted by δ_{rj} (Tu, 2025), c represents the bearing's radial clearance.

The contact forces at the raceway interfaces are calculated according to Hertz contact theory, as follows:

$$\begin{bmatrix} Q_{ij} \\ Q_{oj} \end{bmatrix} = \begin{bmatrix} K_{ci}\delta_{ij}^{3/2} \\ K_{co}\delta_{oj}^{3/2} \end{bmatrix} \tag{31}$$

Thus, the friction force is given by:

$$\begin{bmatrix} F_{ij} \\ F_{oj} \end{bmatrix} = -\mu \begin{bmatrix} Q_{ij}\dfrac{\Delta v_{ij}}{|\Delta v_{ij}|} \\ Q_{oj}\dfrac{\Delta v_{oj}}{|\Delta v_{oj}|} \end{bmatrix} \tag{32}$$

https://doi.org/10.5194/ms-2026-201
Preprint. Discussion started: 20 November 2026
© Author(s) 2026. CC BY 4.0 License.



mechanical sciences DISCUSSIONS

Friction forces on the inner and outer rings in the X and Y directions:

$$\begin{bmatrix} F_{fix} \\ F_{fiy} \end{bmatrix} = \sum_{j=1}^{Z} F_{ij} \begin{bmatrix} \sin\varphi_j \\ \cos\varphi_j \end{bmatrix} \tag{33}$$

$$\begin{bmatrix} F_{fox} \\ F_{foy} \end{bmatrix} = \sum_{j=1}^{Z} F_{oj} \begin{bmatrix} \sin\varphi_j \\ \cos\varphi_j \end{bmatrix} \tag{34}$$

4.4 Dynamic model

To simplify the analysis of complex contact conditions caused by an outer-ring defect, the bearing system is represented by the model in Fig. 6. For the ACBB configuration with a single defect on the outer ring, as illustrated in Fig. 1(a), the resulting contact deformation between the raceway and the *j*-th rolling element can be expressed as:

$$\delta_j = (x_1 - x_2)\cos\varphi_j + (y_1 - y_2)\sin\varphi_j - c - h_{ci} - h_{co} - H_d\cos\alpha \tag{35}$$

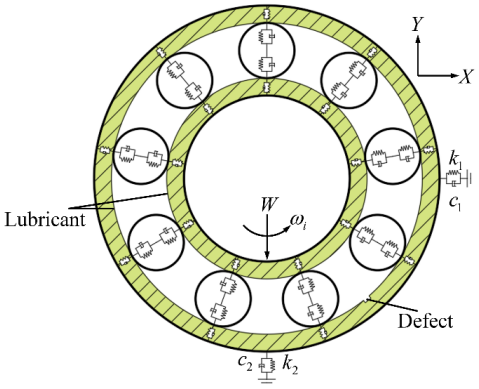


Figure. 6 Schematic of an outer-ring defect in ACBBs

The nonlinear contact-force relationships for the defective ACBB are formulated by resolving the lubrication-influenced Hertz contact load into its X- and Y-direction components.

$$\begin{bmatrix} F_x \\ F_y \end{bmatrix} = \sum_{j=1}^{Z} K_c \delta_j^{\frac{3}{2}} \begin{bmatrix} \cos\alpha_j \cos\varphi_j \\ \cos\alpha_j \sin\varphi_j \end{bmatrix} \tag{36}$$

where F_x and F_y represent the X and Y components of the nonlinear bearing reaction force, respectively. The final contact angle is denoted by α_j, with its calculation method and value referred to Petersen et al. (2015).

The skidding dynamics of ACBBs with a localized outer-ring defect are modeled using Newton's second law in conjunction with Lagrange's equation. The resulting system is described by four-degree-of-freedom dynamic equations, as presented in Eq. (37).

$$\begin{cases} m_1\ddot{x}_1 + c_1\dot{x}_1 + k_1x_1 + F_x + F_{fix} = W_x \\ m_1\ddot{y}_1 + c_1\dot{y}_1 + k_1y_1 + F_y + F_{fiy} = W_y \\ m_2\ddot{x}_2 + c_2\dot{x}_2 + k_2x_2 - F_x - F_{fox} = 0 \\ m_2\ddot{y}_2 + c_2\dot{y}_2 + k_2y_2 - F_y - F_{foy} = 0 \end{cases} \tag{37}$$

where W_x and W_y represent the external loads along the horizontal and vertical axes, respectively. The inner- and outer-ring masses are denoted by m_1 and m_2, respectively.

5. Simulation results and analysis

https://doi.org/10.5194/ms-2026-201
Preprint. Discussion started: 20 November 2026
© Author(s) 2026. CC BY 4.0 License.



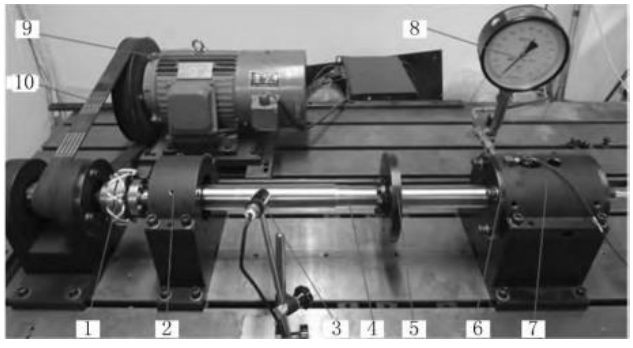
mechanical sciences
DISCUSSIONS

5.1 Experimental validation

The developed ACBB fault formulation is evaluated using the experimental data reported by Zhou et al. (2014). Tests were conducted on an HRB7206AC bearing, whose specifications are listed in Table 2. To reproduce localized raceway damage, a pit with a width of 0.3 mm was fabricated by electrical discharge machining. The test conditions included a preload of 600 N and a shaft speed of 1200 r/min. The experimental setup is presented in Fig. 7.

Table 2. Structure size of bearing.

Notation	Specification	Value
D_i	Inner diameter of the inner race/m	0.03
D_o	Outer diameter of the inner race/m	0.062
d_b	Diameter of roller/m	0.0095
Z	Number of rollers	12
D	Bearing width/m	0.016
α_0	Initial contact angle/°	25



1—Flexible coupling; 2—Left-side bearing housing; 3—Rotational speed sensor; 4—Spindle; 5—Mass disc; 6—Accelerometer; 7—Right-side bearing housing; 8—Hydraulic pressure gauge indicating preload; 9—Drive motor; 10—Power transmission belt.

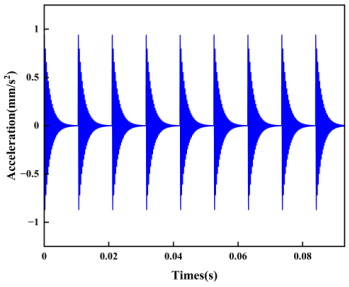
Figure 7. The test rig in the reference

For numerical simulation, the bearing properties listed in Table 2 are used as model inputs. The resulting equations are integrated with the fourth-order Runge-Kutta scheme, using a time increment of $\Delta t = 1\times10^{-4}$ s. The initial displacement conditions are set to $x_0 = 10^{-6}$ mm and $y_0 = 10^{-6}$ mm along the x- and y-axes, respectively. The calculated bearing vibration response is presented in Fig. 8.

https://doi.org/10.5194/ms-2026-201
Preprint. Discussion started: 20 November 2026
© Author(s) 2026. CC BY 4.0 License.



mechanical sciences DISCUSSIONS



(a) Time-domain diagram (b) Envelope spectral plot

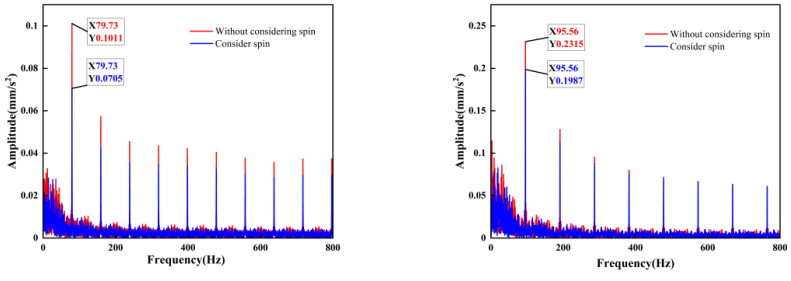
Figure 8. Simulated vibration response of a bearing with an outer-ring defect

The time-domain response has clear periodic impact features, as illustrated in Fig. 8(a). The time intervals between successive impacts are almost consistent, and each impact is followed by oscillations that progressively decay. The predicted waveform is consistent with the experimental observations reported in the literature. For the bearing considered, the theoretical outer-ring fault frequency is $f_o = 97.48$ Hz , while the simulated frequency from the presented model is $f_o = 95.56$ Hz , with an error of 1.9 %.

5.2 Parametric effects on bearing vibration

5.2.1 Effect of spin motion

Numerical analyses are performed to examine how spin motion affects the vibration behavior of defective bearings. The defect size L is 1 mm, the radial loads are specified as $W_x = 600$ N and $W_y = 600$ N , and the speeds are 1000 and 1200 r/min, respectively. The corresponding results are presented in Fig. 9.



(a)1000r/min (b)1200r/min

Figure 9. Effect of spin motion

Under identical operating conditions, the model incorporating spin motion predicts a lower response amplitude than the model without this effect. This result suggests that spin motion suppresses bearing vibrations. As the rotational speed increases, both the fault characteristic frequency and the response amplitude rise, although the response amplitude remains lower when spin motion is considered. This behavior can be attributed to changes in contact kinematics associated with spin motion. The resulting reduction in minimum film thickness increases the film stiffness, thereby enhancing the overall bearing stiffness and improving system stability.

5.2.2 Effect of EHL

The influence of EHL is investigated by comparing bearing responses calculated with and without lubrication effects at various speeds. The defect size L is set to 1 mm, the radial loads are

https://doi.org/10.5194/ms-2026-201
Preprint. Discussion started: 20 November 2026
© Author(s) 2026. CC BY 4.0 License.



mechanical sciences DISCUSSIONS

$W_x = 600$ N and $W_y = 600$ N, and the speeds are 1000, 1200, and 1500 r/min，respectively. The results are presented in Fig. 10.

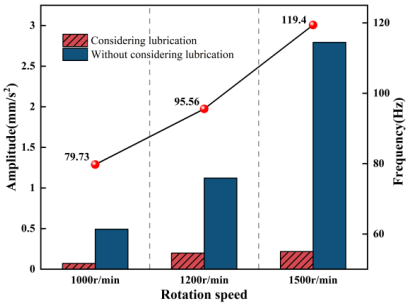
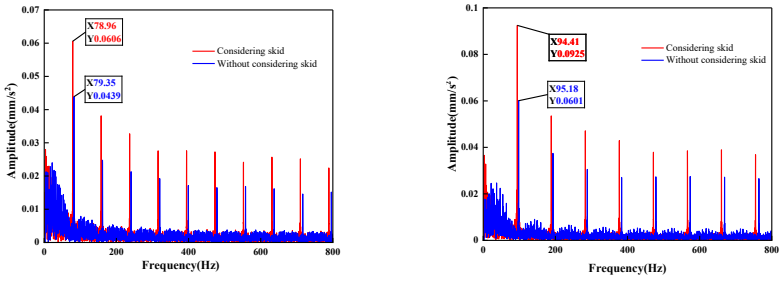


Figure 10. Effect of EHL on bearing vibration response under various speeds

As shown in Fig. 10, increasing the speed raises both the fault vibration frequency and the amplitude. At a given speed, the vibration amplitude of the bearing considering EHL is significantly lower than that without considering it. This is because the lubricant plays a significant regulating role between raceway and the surface. The lubricant forms an oil film through its fluidity and viscosity, altering the rigid contact state. The oil film also moderates velocity variations caused by impacts to some extent. When the bearing is subjected to external excitation that induces vibration, the oil film, which possesses a certain stiffness, can absorb and dissipate part of the vibration energy through its deformation and recovery, thereby effectively reducing the vibration amplitude and improving the operational stability of the bearing.

5.2.3 Effect of skidding

To examine the role played by skidding independently, the vibration of the defective bearing is analyzed without including impact effects. L is 1 mm, the radial loads are $W_x = 600$ N and $W_y = 600$ N, and simulations are performed at speeds of 1000 and 1200 r/min. The calculated result is shown in Fig. 11.



（a）1000r/min （b）1200r/min

Figure 11. Effect of rolling element skidding on bearing vibration response

Fig. 11(a) indicates that the fundamental frequency obtained with skidding is 78.96 Hz, slightly below the value of 79.35 Hz predicted without skidding. This difference is associated with the reduction in effective speed caused by skidding. A comparison of Fig. 11(a) and Fig. 11(b) reveals that the frequency difference becomes more pronounced at higher speeds, since increased rotational speed intensifies skidding at the raceway contact. These results indicate that skidding reduces the fault characteristic frequency. Meanwhile, higher skidding velocity strengthens friction within the contact region, leading to more intense vibration excitation and a greater response amplitude.

5.2.4 Impact effects

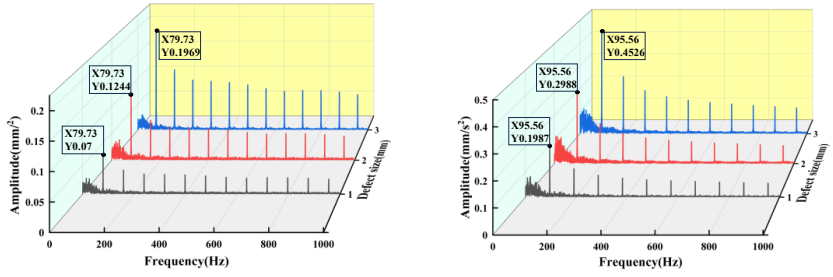
To investigate impact effects on bearing vibration, simulations are conducted at different rotational speeds for a fixed defect size and at different defect sizes for a fixed rotational speed. Fig. 12(a) and 12(b) show the envelope spectra of the defective bearing under EHL at rotational speeds of 1000 and 1200 r/min, respectively. Defect sizes L for the 1 mm, 2 mm, and 3 mm, and radial

https://doi.org/10.5194/ms-2026-201
Preprint. Discussion started: 20 November 2026
© Author(s) 2026. CC BY 4.0 License.



mechanical sciences DISCUSSIONS

loads $W_x = 600$ N and $W_y = 600$ N.



（a）1000r/min （b）1200r/min

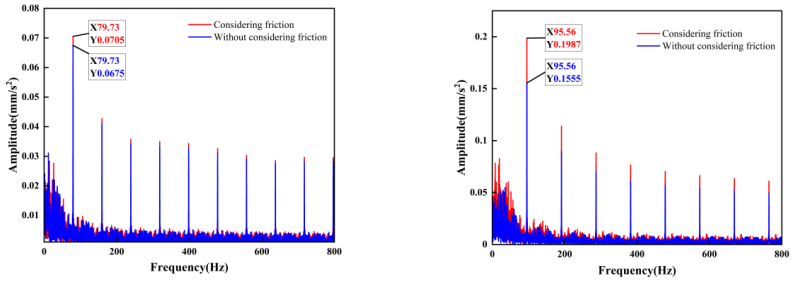
Figure 12. Effect of defect-edge impacts on bearing vibration response

Fig. 12 reveals two distinct trends. With the defect size held constant, higher speeds produce increases in the fault-related characteristic frequency and response. When speed remains unchanged, enlarging the outer-ring defect can raise amplitude, whereas the frequency is unaffected. This behavior reflects the dependence of the characteristic frequency on rotational speed. In addition, a larger defect combined with a higher speed intensifies transient impacts within the damaged region. The resulting excitation force becomes stronger, leading to a greater response and potentially compromising bearing stability.

Compared with Fig. 11, where skidding is considered without defect-edge impacts, the present model accounts for the additional effect of collision at the defect boundary. As the damaged region is traversed, the collision produces a sudden change in velocity, increasing the equivalent motion velocity. Consequently, the predicted fault characteristic frequency exceeds the value obtained when only skidding is considered. This comparison demonstrates that defect-edge impacts modify both the amplitude and the fault characteristic frequency.

5.2.5 Effect of friction

Under EHL, rolling element skidding inevitably introduces friction, which is directly affected by the skidding velocity and contact load. The defect size L is 1mm, the radial loads are $W_x = 600$ N and $W_y = 600$ N, and the speeds are 1000 and 1200 r/min. The result is presented in Fig. 13.



（a）1000r/min （b）1200r/min

Figure 13. Effect of speed

The results in Fig. 13 show that higher speeds lead to increases in both the frequency and amplitude. Incorporating friction into the bearing model also produces a noticeable rise in the predicted amplitude, highlighting the significant influence of friction on bearing vibration.

https://doi.org/10.5194/ms-2026-201
Preprint. Discussion started: 20 November 2026
© Author(s) 2026. CC BY 4.0 License.



mechanical sciences DISCUSSIONS

To further investigate the effect of friction, Fig. 14 presents the different friction on the bearing response. At a constant rotational speed, variations in skidding friction do not alter the fault characteristic frequency. However, the response amplitudes increase with stronger skidding friction, indicating that friction intensifies bearing vibrations and adversely affects the overall dynamic performance of the system.

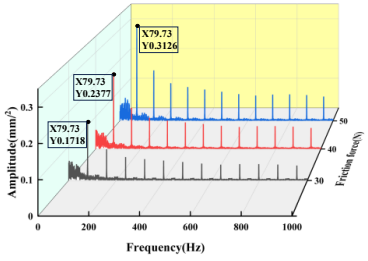


Figure 14. Effect of friction

5.2.6 Effect of radial load

The role of radial loading in the EHL-based vibration response of ACBBs is investigated. All simulations are performed at n=1000 r/min with a defect size of 1 mm. Two loading cases are considered: first, W_x is maintained at 600 N while W_y varies from 600 to 1000 N; second, W_y remains at 600 N while W_x increases over the same range. The result is presented in Fig. 15.

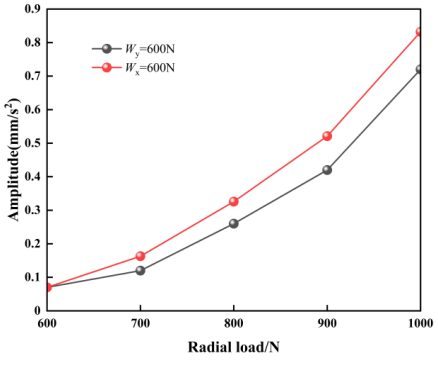


Figure 15. Effect of radial load

Under fixed defect size and speed, a higher radial load strengthens the contact force at the raceway interface, thereby increasing amplitude. For equal radial loading, the Y-direction force exerts a greater influence on the amplitude. As the radial load increases, the amplitude grows more rapidly under the Y-direction load, indicating that the increase in Y-direction load has a more pronounced effect on the amplitude than that in the X-direction load. Moreover, although the increase in load raises the amplitude, it does not alter the fault characteristic frequency.

6. Conclusions

To thoroughly characterize the skidding dynamic behavior of ACBBs operating with an outer-ring defect under realistic service conditions, this study formulates a nonlinear dynamic model that considers spin motion, EHL, and the coupling of skidding and impact effects, and examines its response across various parameters. The main conclusions are drawn:

(1) Spin motion enhances oil film stiffness by altering the kinematics at the raceway interface, thereby increasing its comprehensive stiffness and ultimately reducing its amplitude. EHL, on the other hand, generates an interfacial layer between the contacting surfaces that offers damping and cushioning effects, thereby mitigating bearing oscillations. However, neither alters the bearing's fault characteristic frequency.

(2) Skidding lowers the bearing's fault characteristic frequency. When the velocity variation induced by defect-edge impacts as the rolling element traverses the defective region is considered,

https://doi.org/10.5194/ms-2026-201
Preprint. Discussion started: 20 November 2026
© Author(s) 2026. CC BY 4.0 License.



mechanical sciences
DISCUSSIONS

the element exhibits a noticeable speed increment during its passage through the defect. This leads to an increase in its equivalent motion velocity, thereby resulting in a higher fault characteristic frequency than that obtained when only the skidding effect is considered, together with an increase in amplitude. However, larger defects do not alter the bearing's characteristic fault frequency.

(3) Friction aggravates bearing oscillations. Under fixed defect dimensions and rotational speed, with increasing radial load, the amplitude measured for the bearing rises, whereas the frequency remains unchanged. Raising the rotational speed produces marked increases in the frequency and amplitude.

Code and data availability

The data that support the findings of this study are available from the author.

Author contributions

All the authors participated in the study of the coupled skidding–impact dynamics of angular contact ball bearings with localized outer ring defects under elastohydrodynamic lubrication. XBW wrote the paper and conducted the experiments, LCL was responsible for the overall algorithm verification and the revision of the paper, ZWL was responsible for the drawing of graphics and text as well as the submission of the paper, JMJ established and calculated the dynamic model, ZXW and RGY were responsible for the design and analysis of the vibration model.

Competing interests

The authors affirm that no potential conflicts of interest exist regarding the research, authorship, or publication of this article.

Disclaimer

Publisher's note: Copernicus Publications remains neutral with regard to jurisdictional claims made in the text, published maps, institutional affiliations, or any other geographical representation in this paper. While Copernicus Publications makes every effort to include appropriate place names, the final responsibility lies with the authors. Views expressed in the text are those of the authors and do not necessarily reflect the views of the publisher.

Funding

This work was supported by National Natural Science Foundation of China (No. 51465035, No. 52465013) and the Natural Science Foundation of Gansu Province of China (No. 20JR5RA466).

References

Bao, M., Wang, L., Wang, J., and Zhang, C.: Slipping in cylindrical roller bearings at the simultaneous rotation of inner and outer rings, Tribol. Int., 197, 109767, https://doi.org/10.1016/j.triboint.2024.109767, 2024.

Cao, H., Niu, L., Xi, S., and Chen, X.: Mechanical model development of rolling bearing-rotor systems: a review, Mech. Syst. Signal Process., 102, 37–58, https://doi.org/10.1016/j.ymssp.2017.09.023, 2018.

Dadouche, A. and Kerrouche, R.: Bearing skidding detection for high-speed and aero-engine applications, J. Eng. Gas Turbines Power, 144, 031003, https://doi.org/10.1115/1.4052428, 2022.

Dawoud, M., Beitler, S., and Schwarze, H.: Slip characteristics in cylindrical roller bearings – Part III: Influence of bearing clearance on the roller and set slip, J. Tribol., 145, 021205, https://doi.org/10.1115/1.4055557, 2023.

Evans, R. D., Barr, T. A., Houpert, L., and Boyd, S. V.: Prevention of smearing damage in cylindrical roller bearings, Tribol. Trans., 56, 703–716, https://doi.org/10.1080/10402004.2013.788236, 2013.

Hamrock, B. J. and Dowson, D.: Isothermal elastohydrodynamic lubrication of point contacts: Part III – Fully flooded results, J. Lubr. Technol., 99, 264–275, https://doi.org/10.1115/1.3453074, 1977.

Han, Q., Li, X., and Chu, F.: Skidding behavior of cylindrical roller bearings under time-variable load conditions, Int. J. Mech. Sci., 135, 203–214, https://doi.org/10.1016/j.ijmecsci.2017.11.013, 2018.

Harris, T. A.: An analytical method to predict skidding in thrust-loaded, angular-contact ball bearings, J. Lubr. Technol., 93, 17–24, https://doi.org/10.1115/1.3451511, 1971.

Jiang, Y., Huang, W., Luo, J., and Wang, W.: An improved dynamic model of defective bearings considering the three-dimensional geometric relationship between the rolling element and defect area, Mech. Syst. Signal Process., 129, 694–716,

https://doi.org/10.5194/ms-2026-201
Preprint. Discussion started: 20 November 2026
© Author(s) 2026. CC BY 4.0 License.



mechanical sciences
DISCUSSIONS

https://doi.org/10.1016/j.ymssp.2019.04.056, 2019.
Jain, S. and Hunt, H.: A dynamic model to predict the occurrence of skidding in wind-turbine bearings, J. Phys. Conf. Ser., 305, 012027, https://doi.org/10.1088/1742-6596/305/1/012027, 2011.
Kragelskii, I. V.: Friction and wear, Butterworths, London, UK, 1965.
Lei, C., Gong, B., Jia, X., and Zhao, M.: Influence of spinning on elastohydrodynamic lubrication and film stiffness of angular contact ball bearings, Lubr. Eng., 45, 19–25, 31, https://doi.org/10.3969/j.issn.0254-0150.2020.12.004, 2020.
Lei, C., Song, R., Fan, G., Liu, K., Xue, W., and Li, J.: Vibration characteristics of angular contact ball bearings with local defects considering friction, Tribology, 44, 1355–1365, https://doi.org/10.16078/j.tribology.2023062, 2024.
Lei, C., Song, R., Fan, G., Liu, K., Xue, W., and Li, J.: Time-varying displacement excitation and dynamic modeling of local defects in angular contact ball bearings, J. Beijing Univ. Aeronaut. Astronaut., 51, 753–762, https://doi.org/10.13700/j.bh.1001-5965.2023.0165, 2025.
Li, B., Li, Z., and He, D.: Dynamic modeling and analysis of defective bearings with thorough consideration of fluid-thermal-solid coupling, Mech. Syst. Signal Process., 244, 113765, https://doi.org/10.1016/j.ymssp.2025.113765, 2026.
Li, C., Qin, Y., Wang, Y., and Chen, H.: Vibration analysis of deep groove ball bearings with local defect using a new displacement excitation function, J. Tribol., 142, 121202, https://doi.org/10.1115/1.4048163, 2020.
Li, H., He, Y., Feng, K., Jiang, Z., and Feng, F.: Dynamic modeling of rolling bearing local fault considering time-varying excitation, Acta Aeronaut. Astronaut. Sin., 43, 625176, https://doi.org/10.7527/S1000-6893.2021.25176, 2022.
Li, J., Lei, C., Gong, B., Cui, P., and Jia, X.: Modeling and analysis of the composite stiffness for angular contact ball bearings, Shock Vib., 2020, 8832750, https://doi.org/10.1155/2020/8832750, 2020.
Shang, Z., Pang, H., Gao, M., and Liu, J.: Modeling and analysis of local failure gradual dynamics of rolling bearing inner ring, J. Mech. Strength, 45, 778–784, https://doi.org/10.16579/j.issn.1001.9669.2023.04.003, 2023.
Luo, M. L., Guo, Y., and Wu, X.: Dynamic modeling of double-impact phenomenon of outer-race spalling defects in ball bearings considering impact force, J. Vib. Shock, 38, 48–54, https://doi.org/10.13465/j.cnki.jvs.2019.14.007, 2019.
Niu, L., Cao, H., He, Z., and Li, Y.: Dynamic modeling and vibration response simulation for high-speed rolling ball bearings with localized surface defects in raceways, J. Manuf. Sci. Eng., 136, 041015, https://doi.org/10.1115/1.4027334, 2014.
Patel, V. N., Tandon, N., and Pandey, R. K.: A dynamic model for vibration studies of deep groove ball bearings considering single and multiple defects in races, J. Tribol., 132, 041101, https://doi.org/10.1115/1.4002333, 2010.
Petersen, D., Howard, C., and Prime, Z.: Varying stiffness and load distributions in defective ball bearings: analytical formulation and application to defect size estimation, J. Sound Vib., 337, 284–300, https://doi.org/10.1016/j.jsv.2014.10.004, 2015.
Qin, Y., Li, C., Cao, F., and Chen, H.: A fault dynamic model of high-speed angular contact ball bearings, Mech. Mach. Theory, 143, 103627, https://doi.org/10.1016/j.mechmachtheory.2019.103627, 2020.
Tu, W. B., Zhang, G. Y., Yuan, X. W., Luo, Y., Wang, J. M., and Wang, H.: Review and prospects of skidding in rolling bearings, Journal of Mechanical Strength, 46, 484–496, https://doi.org/10.16579/j.issn.1001.9669.2024.02.030, 2024.
Tu, W., Yu, W., Shao, Y., and Yu, Y.: A nonlinear dynamic vibration model of cylindrical roller bearing considering skidding, Nonlinear Dyn., 103, 2299–2313, https://doi.org/10.1007/s11071-021-06238-0, 2021.
Wang, Y., Wang, W., Zhang, S., and Zhao, Z.: Investigation of skidding in angular contact ball bearings under high speed, Tribol. Int., 92, 404–417, https://doi.org/10.1016/j.triboint.2015.07.021, 2015.
Wen, C., Meng, X., Fang, C., Gu, J., Xiao, L., and Jiang, S.: Dynamic behaviors of angular contact ball bearing with a localized surface defect considering the influence of cage and oil lubrication, Mech. Mach. Theory, 162, 104352, https://doi.org/10.1016/j.mechmachtheory.2021.104352, 2021.

https://doi.org/10.5194/ms-2026-201
Preprint. Discussion started: 20 November 2026
© Author(s) 2026. CC BY 4.0 License.



mechanical sciences
DISCUSSIONS

548 Wu, X., Qin, Y., Luo, J., Wang, S., and Chen, B.: Fault dynamic model of high-speed rolling
549 bearing by a compound displacement excitation function considering the effect of defect
550 roughness, Mech. Mach. Theory, 177, 105061,
551 https://doi.org/10.1016/j.mechmachtheory.2022.105061, 2022.
552 Xu, C., Fan, Q., Zhang, Q., Tong, Y., Wang, S., and Wu, T.: Vibration-based wear evolution
553 characterisation of lubricated rolling-sliding contact, Lubricants, 13, 78,
554 https://doi.org/10.3390/lubricants13020078, 2025.
555 Yan, C., Kang, J., Yuan, H., Wu, L., and Wei, Y.: Dynamic modeling for local defect
556 displacement excitation in rolling bearing systems under elasto-hydrodynamic lubrication
557 and slip, J. Vib. Shock, 37, 56–64, https://doi.org/10.13465/j.cnki.jvs.2018.05.009, 2018.
558 Yan, P., Yan, C., Wang, K., Wang, F., and Wu, L.: 5-DOF dynamic modeling of rolling bearing
559 with local defect considering comprehensive stiffness under isothermal
560 elastohydrodynamic lubrication, Shock Vib., 2020, 9310278,
561 https://doi.org/10.1155/2020/9310278, 2020.
562 Zhang, F., Zhang, Y., Guan, J., Tian, J., and Wang, Y.: Fault dynamic modeling and
563 characteristic parameter simulation of rolling bearing with inner ring local defects, Shock
564 Vib., 2021, 5077366, https://doi.org/10.1155/2021/5077366, 2021.
565 Zhao, Y., Ma, Z., and Zi, Y.: Skidding and spinning investigation for dry-lubricated angular
566 contact ball bearing under combined loads, Friction, 11, 1987–2007,
567 https://doi.org/10.1007/s40544-022-0703-9, 2023.
568 Zhou, Z., Zhu, Y. S., Yan, K., and Zhang, Y. Y.: A seven-degree-of-freedom dynamic model of
569 angular contact ball bearings considering defect factors, Comput. Integr. Manuf. Syst., 20,
570 2836–2842, https://doi.org/10.13196/j.cims.2014.11.023, 2014.
571